BIOCHEMISTRY
including biophysical chemistry & molecular biology

Article

pubs.acs.org/biochemistry

The Structure of the Holo-Acyl Carrier Protein of *Leishmania major* Displays a Remarkably Different Phosphopantetheinyl Transferase Binding Interface

Ambrish Kumar,[†] Richa Arya,[‡] Pinakin K. Makwana,[†] Rohit Singh Dangi,[†] Usha Yadav,[†] Avadhesha Surolia,[§] Suman Kundu,[‡] and Monica Sundd*[,†]

[†]National Institute of Immunology, Aruna Asaf Ali Marg, New Delhi 110 067, India

[‡]Department of Biochemistry, University of Delhi South Campus, Benito Juarez Road, New Delhi 110 021, India

[§]Molecular Biophysics Unit, Indian Institute of Science, Bangalore 560 012, India

Supporting Information

ABSTRACT: The genome of *Leishmania major* encodes a type II fatty acid biosynthesis pathway for which no structural or biochemical information exists. Here, for the first time, we have characterized the central player of the pathway, the acyl carrier protein (LmACP), using nuclear magnetic resonance (NMR). Structurally, the LmACP molecule is similar to other type II ACPs, comprising a four-helix bundle, enclosing a hydrophobic core. Dissimilarities in sequence, however, exist in helix II (recognition helix) of the protein. The enzymatic conversion of apo-LmACP into the holo form using type I (*Escherichia coli* AcpS) and type II (Sfp type) phosphopantetheinyl transferases (PPTs) is relatively slow. Mutagenesis studies underscore the importance of the residues present at the protein−protein interaction interface of LmACP in modulating the activity of PPTs. Interestingly, the cognate PPT for this ACP, the *L. major* 4′-phosphopantetheinyl transferase (LmPPT), does not show any enzymatic activity toward it, though it readily converts other type I and type II ACPs into their holo forms. NMR chemical shift perturbation studies suggest a moderately tight complex between LmACP and its cognate PPT, suggesting inhibition. We surmise that the unique surface of LmACP might have evolved to complement its cognate enzyme (LmPPT), possibly for the purpose of regulation.

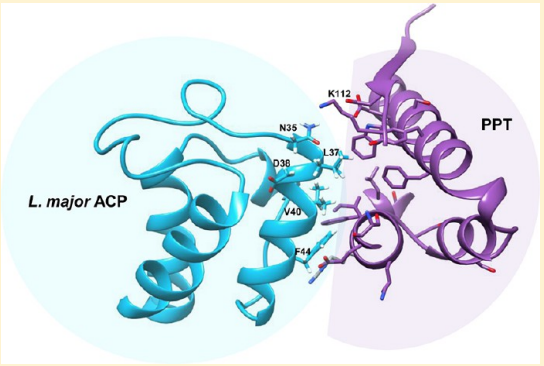

Leishmaniasis is an important tropical disease that threatens millions of lives worldwide. The severity of the infection varies with species, ranging from cutaneous lesions to fatal systemic infections (visceral leishmaniasis). The disease has raised heightened concern lately, because of the surge in multidrug resistant strains.[1,2] There are no licensed vaccines available to date, and chemotherapy still remains the ultimate choice.[3] Hence, there is pressing need to identify new targets for intervention.

Notably, the surface of *Leishmania* spp. is rich in glycosphingolipids, and a marked change in the lipid content of the parasite occurs in the drug resistant species.[4] Moreover, the amastigote stage (blood stage) of the parasite relies on the β-oxidation of fatty acids for energy generation, classifying the fatty acid metabolism as a suitable target for drug design.[5−8] Though a major fraction of the lipid requirement in the amastigote stage is met by the host, a functional machinery for *de novo* synthesis and remodeling of fatty acids is also retained in the parasite.[9] On the basis of genome sequence, two distinct pathways for fatty acid synthesis (FAS) coexist, (a) a type II pathway and (b) an elongase pathway.

Most of the biochemical information about trypanosomatids comes from the studies on *Trypanosoma*, a close relative of *Leishmania*. Speculation is rife that the primer for the elongase pathway, i.e., butyryl-CoA, is supplied by the type II fatty acid biosynthesis pathway of *Trypanosoma brucei*, as the elongase pathway cannot function *de novo*.[10] Studies of the conditional knockouts of the acyl carrier protein (ACP), an important component of the fatty acid machinery, have shown that in the absence of ACP, cell death occurs in the bloodstream form, underscoring the importance of fatty acid biosynthesis for survival.[10] Interestingly, the amino acid sequence of *Leishmania major* ACP is ∼96% identical to that of *T. brucei* (excluding the signal peptide of ∼70 amino acids).[10]

The type II fatty acid biosynthesis pathway of several other microorganisms has been studied and in some pathogens has been regarded as a target for drug design, because of its dissimilarities with the type I fatty acid biosynthesis pathway of the host.[11,12] An indispensable component common to both the

Received: October 1, 2014
Revised: August 14, 2015
Published: August 20, 2015

DOI: 10.1021/acs.biochem.5b00394
Biochemistry 2015, 54, 5632−5645

pathways is the acyl carrier protein (ACP), which interacts with the enzymes of the fatty acid machinery. ACP is an independent component of the type II pathway with two distinct functions when loaded with an acyl chain (a) communicating with the catalytic enzymes while delivering the growing acyl chain to their active site and (b) protecting the acyl chain in its core from the hydrophilic environment during transport.[13] In the type I pathway, it exists as an integral domain of one single multidomain, multifunctional fatty acid synthase (FAS). Intriguingly, ACPs of the type I and II pathways share a very similar fold, and the type I ACP domains can act as a substrate for the type II bacterial fatty acid synthase enzymes.[14]

The process of fatty acid synthesis occurs in two stages, (a) initiation and (b) elongation.[15] The initiation steps involve the carboxylation of acetyl-CoA to malonyl-CoA, in the presence of acetyl-CoA carboxylase, and the subsequent transfer of the malonyl group from CoA to holo-ACP in the presence of malonyl-CoA:ACP transacylase. Prior to this step, the post-translational modification of the apo-ACP by the transfer of the phosphopantetheine moiety from coenzyme A to a conserved Ser residue is caused by the enzyme 4′-phosphopantetheinyl transferase (PPT). In the subsequent step, one molecule of acetyl-CoA condenses with malonyl-ACP in the presence of β-ketoacyl-ACP synthase III to form acetoacetyl-ACP, which enters the elongation cycle. The first product of the elongation cycle is butyryl-ACP, followed by the addition of two carbons to the chain per elongation cycle, resulting in longer chain acyl-ACPs.

Apart from fatty acid biosynthesis, ACP plays a pivotal role in polyketide synthesis,[16,17] oligosaccharide,[18] biotin, and non-ribosomal peptide synthesis.[19,20] ACP has been well-characterized in *Escherichia coli*,[21−23] spinach,[24] *Plasmodium falciparum*,[25−27] rat,[14,28] *Vibrio harveyi*,[29] and others.

ACP molecules display a low level of sequence identity of ∼20% yet share a very similar topology, four helices surrounding a hydrophobic cavity. A Ser residue at position 36 is conserved within a "DSL" motif. Structural studies of the ACP−enzyme complexes have shown that the majority of the interactions of the ACP molecule are governed by loop I, helix II (recognition helix), loop II, and helix III, which form a contiguous surface.[30,31]

As a first step toward understanding the function of the type II fatty acid biosynthesis pathway of *L. major*, we have structurally characterized its acyl carrier protein and compared it with other type II ACPs. Its unusual PPT binding surface guided us to follow its interaction with various groups of PPTs, using biochemical and biophysical techniques. Our studies shed light on the role of the residues present at the protein−protein interaction interface of ACP, in modulating the catalytic activity of PPTs.

EXPERIMENTAL PROCEDURES

Cloning, Expression, and Purification. Cloning, expression, and purification of ACPs from *L. major* (LmACP), *E. coli*, *P. falciparum*, *Mycobacterium tuberculosis*, and *Homo sapiens* were conducted in *E. coli* as described previously.[32] *L. major* 4′-phosphopantetheinyl transferase (LmPPT, UniProt entry Q4QCW3) was also purified similarly. The proteins were overexpressed by inducing with 0.4 mM isopropyl β-D-1-thiogalactopyranoside. Cells were harvested and sonicated, followed by Ni^{2+}-NTA chromatography. The bound proteins were eluted with 50−200 mM imidazole.

Holo-ACP was synthesized *in vitro* using *Bacillus subtilis* phosphopantetheinyl transferase (Sfp), apo-ACP, and coenzyme A, using a modified protocol of Lambalot and Walsh.[33] Sfp was expressed and purified separately using ion exchange chromatography. Uniformly labeled [^{1}H,^{15}N,^{13}C]apo-ACP was prepared by growing *E. coli* in M9 medium containing $^{15}NH_4Cl$ (1 g/L) and ^{13}C glucose (2 g/L). The N-terminal His tag was removed by thrombin cleavage using immobilized thrombin. Single-site mutations were introduced using a site-directed mutagenesis approach and purified in a manner analogous to that used for the wild-type protein.

NMR Data Acquisition. NMR samples comprised uniformly labeled [^{1}H,^{15}N,^{13}C]protein, in 20 mM sodium phosphate buffer (pH 6.0), 100 mM NaCl, 2 mM DTT, 0.5% sodium azide, 90% H_2O, and 10% D_2O. A protein concentration of 1 mM was used throughout.

Two- and three-dimensional NMR experiments, viz., $^1H^{15}N$ HSQC, $^1H^{15}N$ TOCSY, HNCACB, CBCAcoNH, CCcoNH, and HNcoCA, were acquired on a Bruker Avance III 700 MHz NMR spectrometer, installed at the National Institute of Immunology (New Delhi, India), equipped with a triple-resonance cryogenic TCI probe. NMR data were processed on a workstation with Red Hat Enterprize Linux 5.0, using NMRDraw/NMRPipe,[34] and analyzed using Sparky[35] and CARA.[36] Experiments were performed at 298 K throughout. The data were multiplied by a phase-shifted sinebell apodization function in all dimensions.

$^1H^{15}N$ HSQC spectra were acquired using 1024 data points in the t_2 dimension and 512 data points in the t_1 dimension. $^1H^{15}N$ HSQC-TOCSY experiments were conducted using a mixing time of 80 ms, with 1024 (t_3) × 72 (t_1) × 48 (t_2) data points. Three-dimensional experiments, viz., CBCAcoNH, HNCACB, and CCcoNH, were performed with 1024 (t_3) × 36 (t_1) × 24 (t_2) data points. In all cases, the data were linear-predicted in the forward direction for up to half the number of experimental points in the indirect dimensions. $^{15}N^{13}C$ spectra were indirectly referenced using a chemical shift standard, sodium 2,2-dimethyl-2-silapentane-5-sulfonate (DSS).[37] Methanol was used as an external standard for temperature measurements.[38]

^{15}N T_1, ^{15}N T_2, and $^{15}N\{^1H\}$ NOE relaxation experiments were performed on an Avance III 700 MHz Bruker NMR spectrometer at 298 K. In the case of T_1 and T_2 measurements, 24 transients were acquired per experiment, and a total of 256 × 2048 complex points were acquired in the $t_1 \times t_2$ dimensions. ^{15}N T_1 relaxation delays of 0.01, 0.02, 0.04, 0.08, 0.16, 0.32, 0.64, 0.96, and 1.28 s were used with the inversion recovery pulse sequence. ^{15}N T_2 relaxation rates were measured using the Carr−Purcell−Meiboom−Gill (CPMG) pulse sequence with relaxation delays of 0.01, 0.03, 0.05, 0.07, 0.09, 0.11, 0.13, 0.15, 0.17, 0.19, 0.21, 0.23, and 0.25 s. NOE measurements were performed using 32 transients per t_1 experiment with 2048 and 128 points in the t_2 and t_1 dimensions, respectively. A recovery delay of 2.5 s was used throughout.

Data Analysis. *Chemical Shift Perturbations.* Changes in HN have been reported as average chemical shifts ($\Delta\Delta\delta_{HN}$) derived from eq 1[39]

$$\Delta\Delta\delta_{HN} = [(\Delta_{HN})^2 + (\Delta N/5)^2]^{1/2} \quad (1)$$

where Δ_{HN} and ΔN are the changes in the proton and nitrogen dimensions, respectively.

One standard deviation has been used as a cutoff to demarcate significant chemical shift change.

Relaxation Data Analysis. The relaxation data were analyzed using Sparky.[35] Intensities of the amides were obtained by measuring the heights of the peaks in the spectra, and the T_1

DOI: 10.1021/acs.biochem.5b00394
Biochemistry 2015, 54, 5632−5645

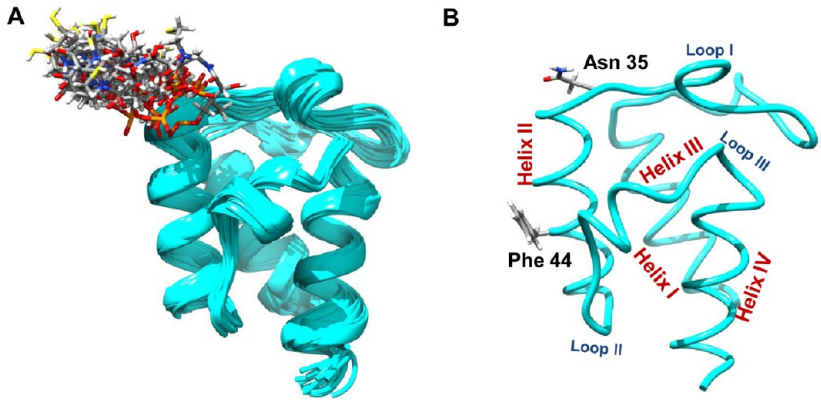

Figure 1. Solution structure of the holo-acyl carrier protein of *L. major*. (A) The 20 lowest-energy conformers obtained by superposition of the backbone of the secondary structural elements are shown. The phosphopantetheine moiety is displayed as sticks. (B) The lowest-energy structure is shown as licorice, displaying the two residues important for its interaction with PPTs. This figure was prepared using Chimera.[57]

and T_2 values were determined from the nonlinear regression of the single-exponential decays. A Sparky2rate script (http://xbeams.chem.yale.edu/~loria/sparky2rate, P. J. Loria, Yale University, New Haven, CT) based on the CURVEFIT software (A. G. Palmer III, Columbia University, New York, NY) was used to translate the relaxation time from the duplicate spectra into relaxation rates and to calculate standard deviations. The $^{15}N\{^1H\}$ heteronuclear steady-state NOE was calculated from the I_{sat}/I_{unsat} ratio, where I_{sat} and I_{unsat} are the peak intensities in the spectra collected with and without proton saturation, respectively. Uncertainties in measurements were derived from independently acquired duplicate spectra.

^{15}N relaxation data were analyzed using FAST-Modelfree,[40] by applying the extended Model-free approach. An isotropic model for rotational diffusion was used. χ^2 testing was used to confirm the goodness of fit. The five models used to describe the spin relaxation data were as follows: model 1, S^2; model 2, S^2 and τ_e; model 3, S^2 and R_{ex}; model 4, S^2, τ_e, and R_{ex}; model 5, S^2, τ_e, and S_f^2. S^2 is the order parameter, with values between 0 and 1, used to fit the amplitude of internal motions on the picosecond to nanosecond time scale. S_f^2 is the order parameter for fast motions, and τ_e is the effective correlation time for internal motions. R_{ex} represents chemical/conformational exchange for the microsecond to millisecond motions.

Structure Determination. Structures were determined using CNS (Crystallography & NMR System version 1.3)[41] based on the NOESY restraints obtained from 3D $^1H^{15}N$ NOESY-HSQC, 3D $^1H^{13}C$ NOESY-HSQC aliphatic, and 3D $^1H^{13}C$ NOESY-HSQC aromatic experiments. The dihedral angle restraints obtained from HNHA/TALOS+ and hydrogen bond restraints from hydrogen−deuterium exchange experiments were also used as input for structure calculation.

Matrix-Assisted Laser Desorption Ionization Time-of-Flight (MALDI-TOF) Analysis. Samples were desalted using C18 ZipTips and eluted with 50% acetonitrile, containing 0.1% TFA. The samples were mixed with an equal volume of matrix (α-cyano-4-hydroxycinnamic acid) and analyzed on a model 4800 MALDI-TOF analyzer.

PPT Assay. The conversion of apo- to holo-ACP was followed by incubating 40 μM apo-ACP, 2 μM Sfp/10 μM LmPPT, 0−100 μM CoA, 2 mM $MgCl_2$, 2 mM DTT, and 50 mM Tris-HCl (pH 8.0). The samples were incubated for 1 h in the case of Sfp and 3−8 h for the LmPPT assay at 37 °C. The extent of conversion was qualitatively monitored on a 12% Native-PAGE gel, as the holo form migrated faster than the apo form. Similarly, the mutants containing the N35D mutation migrated ahead of wild-type LmACP, because of the presence of an additional negative charge. For quantitative kinetic measurements, holo-ACP formed during the assay was monitored using a modified high-performance liquid chromatography (HPLC) method.[42,43] The enzymatic reaction was conducted as described and terminated by the addition of 50 mM EDTA. A 15 μL sample of the assay solution was injected onto a Symmetry C18-5 μm (4.6 mm × 250 mm) column (reversed phase), pre-equilibriated with 0.1% trifluoroacetic acid. The column was eluted with a linear gradient of 0 to 80% acetonitrile in 0.1% trifluoroacetic acid, and the absorbance was monitored at 220 nm. The identity of the HPLC peaks was also confirmed by MALDI-TOF mass spectrometry. In the HPLC chromatogram, the holoprotein eluted prior to the apoprotein, in approximately 20−21 min. The proportion of holo-ACP formed during the assay was estimated by measuring the peak area (integral) for holo-ACP and dividing this value by the sum of the area for apo- and holo-ACP elution peaks, at each coenzyme A concentration.

RESULTS

The *L. major* Holo-Acyl Carrier Protein (LmACP) Displays a Four-Helix Bundle Architecture. The 20 lowest-energy structures of the holo-acyl carrier protein of *L. major* obtained by multidimensional NMR spectroscopy are shown in Figure 1A. The backbone chemical shift assignments were obtained by acquiring triple-resonance NMR experiments, HNCACB, CBCAcoNH, HNCA, HNcoCA, etc.[32] The side chain chemical shift assignments were derived from CCcoNH-TOCSY and HCCH-TOCSY experiments. The NOESY constraints were obtained from ^{13}C-edited NOESY, as well as ^{15}N-edited NOESY experiments. A total of 1407 unique NOE distance restraints, 44 hydrogen bond restraints, and 109 dihedral angle restraints were used for structure determination as illustrated in Table S1. A majority of the ϕ angles were obtained from the HNHA experiment and the ψ angles from TALOS+.[44]

The structure of the holo-LmACP molecule was determined using CNS[41] (Crystallography & NMR System). A total of 200 structures were generated, of which the 20 lowest-energy superimposed structures were submitted to the Protein Data Bank as entry 2M5R. All experimental NMR restraints were satisfied, with no major NOE restraint violations. In the structures, most of the residues have ϕ and ψ angles that fall within the favorable regions of the Ramachandran plot. The

DOI: 10.1021/acs.biochem.5b00394
Biochemistry 2015, 54, 5632−5645

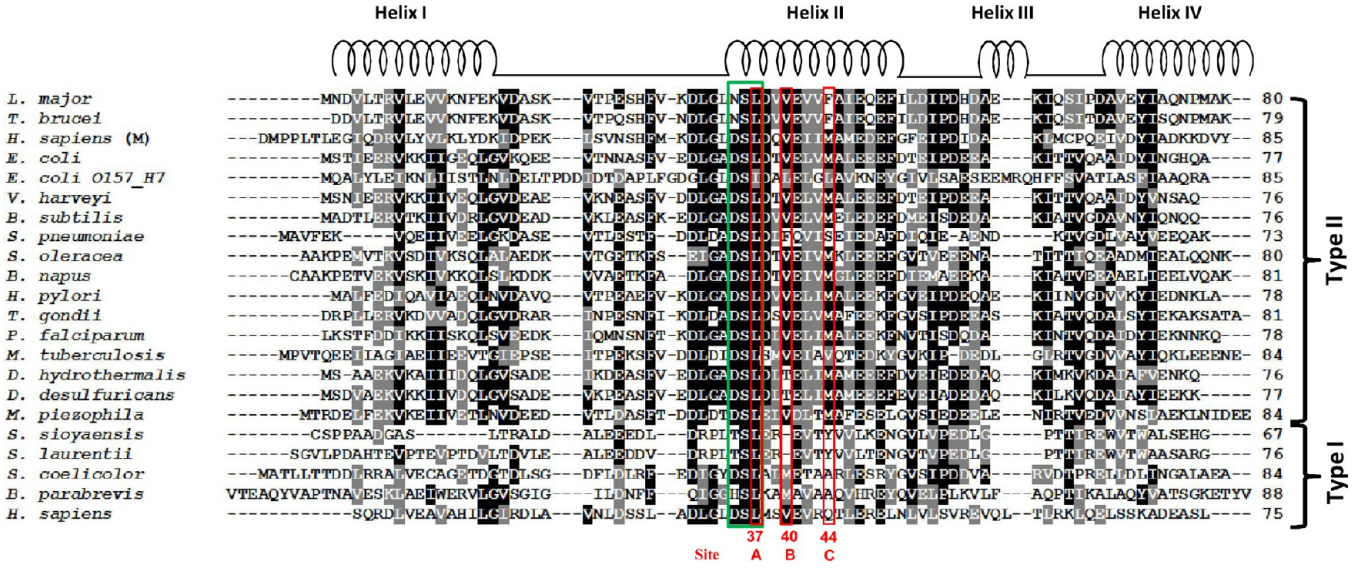

Figure 2. Comparison of the LmACP sequence with other carrier proteins. A multiple-sequence alignment of LmACP with other type I and type II ACPs is shown, along with the secondary structural elements. Positions 37, 40, and 44 are highlighted with a red box. The DSL motif is highlighted with a green box. (M) indicates the protein is a type II ACP, mitochondrial in origin.

average root-mean-square deviation (rmsd) from the lowest-energy structure (backbone) for all the residues was 0.85 Å and that of heavy atoms (C′, C_α and N) 1.24 Å. The average rmsd for the backbone atoms over the four helices was 0.54 Å.

The LmACP molecule is a four-helix bundle protein, comprising helices α-I (residues 1−15), α-II (residues 35−49), α-III (residues 56−60), and α-IV (residues 65−79), that enclose a hydrophobic cavity as shown (Figure 1B). Three well-defined loops connect the four helices; loop I, between helices I and II, loop II, between helices II and III, and loop III between helices III and IV. Loops II and III are relatively short compared to loop I. The residues in the text have been numbered in accordance with *E. coli* ACP structure (PDB entry 1T8K). Hence, the numbering in this work differs by one residue from that of PDB entry 2M5R; i.e., Ser 36 in the text corresponds to Ser 37 in the PDB entry.

Structurally, the LmACP backbone is similar to other type II ACPs. The lowest-energy NMR structure of LmACP displays rmsd values of 2.29 Å with the backbone of *E. coli* (PDB entry 1T8K), 2.12 Å with *P. falciparum* ACP (PDB entry 2FQ0), and 2.58 Å with *H. sapiens* mitochondrial ACP (PDB entry 2DNW), as shown in Figure S1A−C.

In conformity with other type II ACPs, a Ser is conserved at position 36, which undergoes post-translational modification by the covalent attachment of a phosphopantetheine group derived from coenzyme A, in the presence of a 4′-phosphopantetheinyl transferase (PPT) (Figure 2).

The LmACP Backbone Displays Picosecond to Nanosecond Time Scale Dynamics, Akin to Other Carrier Proteins. ^{15}N T_1, T_2, and $^{15}N\{^1H\}$ steady-state NOE values were measured for LmACP at 25 °C. A total of 74 cross-peaks were identified in the HSQC spectrum, of which 67 non-overlapping well-resolved peaks were selected for further analysis. The calculated R_1, R_2, and NOE values for the amides are shown in Figure S2A−C.

The raw data from the relaxation experiments were fitted to the extended Model-free formalism developed by Lipari and Szabo[45] using FAST-Modelfree.[40] An overall global isotropic correlation time of 6.64 ns was determined for holo-LmACP at 25 °C. Residues that showed significant resonance overlap were excluded from the analysis. The model with the fewest parameters that gave a statistically significant χ^2 value was selected. The generalized NH order parameters obtained from the Model-free analysis displayed values between 0.65 and 0.9 for most of the residues, as shown in Figure S2D, suggesting picosecond to nanosecond motions. Nearly all the residues could be fitted to model 1, using Model-free approach, except Asp 56 and His 57, which required an R_{ex} term, and displayed the best fit using model 3, as illustrated in Figure S2E.

Residues in Helix II of LmACP Are Remarkably Different from Those of Other Type II ACPs. Structural comparison of LmACP with other type II ACPs highlights major differences in the residues of helix II, at sites that interact with PPT. LmACP lacks the conserved Asp at position 35 (Figure 2). Likewise, a Met at position 44 is replaced with a Phe in LmACP. Both residues are crucial for the interaction of ACP with PPT.[46]

LmACP Does Not Interact with the Bacterial Group I, 4′-Phosphopantetheinyl Transferase. Heterologous expression of LmACP in *E. coli* yields ∼100% apoprotein. Other type II ACPs, i.e., *E. coli*,[47] *P. falciparum*,[48] spinach,[49] and others,[50] are expressed in two or more forms: apo form, holo form, and the acyl intermediates, as the latter serve as a substrate for the group I 4′-phosphopantetheinyl transferase AcpS, present in *E. coli*.

To dissect the contribution of Asn 35 and Phe 44, present in LmACP, in modulating its interaction with AcpS, the two residues were mutated to the corresponding residues in *E. coli* ACP, singly (N35D and F44M) as well as in combination (N35D +F44M). Figure 3A shows the helical wheel projections for helix II of *E. coli* ACP and LmACP, highlighting the residues (in red) that were mutated. *E. coli* AcpS was able to convert ∼17% of the double mutant N35D+F44M into holo-LmACP (Figure 3B, lane 4), while the wild-type LmACP and single mutants N35D and F44M were expressed predominantly as the inactive apo form in *E. coli*, with 0−1% conversion as shown in Figure 3B (lanes 1−3). The percentage conversion was determined by HPLC analysis. Panels A and B of Figure S3 display the HPLC C18 reverse phase chromatogram for the Ni^{2+}-affinity purified N35D and N35D +F44M mutants, respectively, upon heterologous expression in *E. coli*.

DOI: 10.1021/acs.biochem.5b00394
Biochemistry 2015, 54, 5632−5645

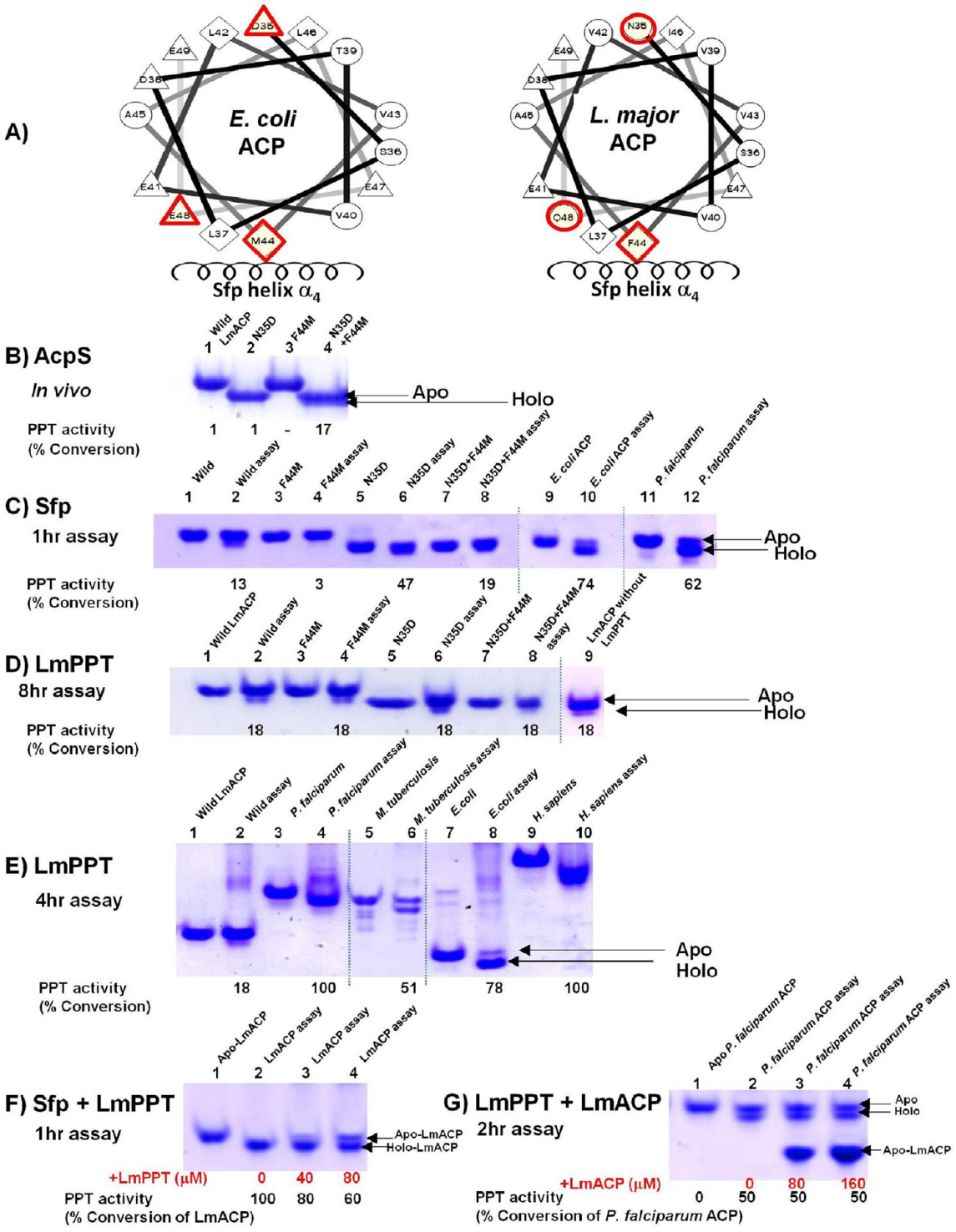

Figure 3. Enzymatic conversion of apo- to holo-ACP. (A) Helical wheel projections of helix II of LmACP and *E. coli* ACP, displaying the residues mutated (colored red) in LmACP to the *E. coli* sequence. On a 12% Native-PAGE gel, (B) conversion of the wild type and mutants of LmACP by AcpS (during heterologous expression), followed by Ni^{2+} affinity chromatography, (C) *in vitro* conversion of various ACPs using *B. subtilis* Sfp, (D) *in vitro* conversion of LmACP and its mutants using LmPPT (the assay was conducted for 8 h in LmPPT using LmACP as a substrate), (E) *in vitro* conversion of heterologous ACPs (type I and type II) using LmPPT, (F) *in vitro* conversion of LmACP by Sfp in the presence of LmPPT, and (G) *in vitro* conversion of *P. falciparum* ACP by LmPPT in the presence of LmACP. A separate lane in a separate gel is shown by a dotted line. The percent conversion was calculated using the modified HPLC method as described.

Enzymatic Conversion of LmACP with *B. subtilis* Sfp Is Relatively Slow. *B. subtilis* Sfp displays broad substrate specificity and converts most known ACPs into their active form. As shown on a 12% Native-PAGE gel (Figure 3, lanes C1−C8), 13% of the wild type, 3% of F44M, 47% of N35D, and 19% of N35D+F44M could be converted to holo-LmACP by incubation with Sfp *in vitro* over a period of 1 h at 37 °C, using 50 μM CoA, 2 μM Sfp, and 40 μM ACP. Under the same assay

DOI: 10.1021/acs.biochem.5b00394
Biochemistry 2015, 54, 5632−5645

conditions, *E. coli* ACP showed 74% conversion, *P. falciparum* ACP 62% (Figure 3, lanes C9−C12), and *M. tuberculosis* ACP 61% conversion (data not shown). Panels C−F of Figure S3 display the HPLC C18 reverse phase chromatograms for the apo and holo forms of wild-type LmACP, N35D, N35D+F44M, and *E. coli* ACP after the Sfp assay, respectively. Longer incubation with Sfp resulted in the complete conversion of LmACP, as confirmed by MALDI-TOF mass spectrometry (Figure S4B).

Kinetic measurements were taken on wild-type LmACP, the single mutants N35D, F44M, and F44A, the double mutants N35D+F44M and N35D+Q48E, triple mutant N35D+F44M +Q48E of LmACP, *E. coli* ACP, the M44F mutant of *E. coli* ACP, *P. falciparum* ACP, and *M. tuberculosis* ACP, using Sfp. The Michaelis−Menten constant K_M was determined by varying the coenzyme A concentration between 0 and 100 μM, using 2 μM Sfp, and a fixed concentration of apo-ACP (40 μM). Kinetic constants were obtained by performing hyperbolic Michaelis−Menten fits to the raw data using Graphpad Prism version 6.0 for Windows (GraphPad Software, La Jolla, CA). The LmACP F44A mutant failed to convert to the holo form even after incubation for 4 h. In other LmACP mutants, a major difference was observed in the V_{max}. As illustrated in Figure 4, the lowest V_{max} was observed for mutant F44M and the highest for N35D. The increase in V_{max} upon mutation of Asn 35 to an Asp was compensated by the decrease upon mutation of Phe 44 to a Met in the double mutant N35D+F44M. As a consequence, the enzyme kinetic curve (reaction rate vs substrate concentration) for the double mutant N35D+F44M was similar to that of the wild-type protein. The k_{cat} values were in the following order: F44M < wild type < N35D+F44M+Q48E < N35D+F44M < N35D+Q48E < N35D < *M. tuberculosis* ACP < *E. coli* ACP < *P. falciparum* ACP (as illustrated in Figure 4 and Table 1). In the double mutant N35D+Q48E, the k_{cat} of Sfp was higher than that of wild-type LmACP but lower than that of the N35D mutant. In the triple mutant N35D+F44M+Q48E, the V_{max} dropped to 0.13 μmol/min. An *E. coli* ACP mutant M44F was also designed and displayed a K_M similar to that of the wild-type *E. coli* ACP, though the V_{max} decreased drastically, as shown in Figure 4 and Table 1.

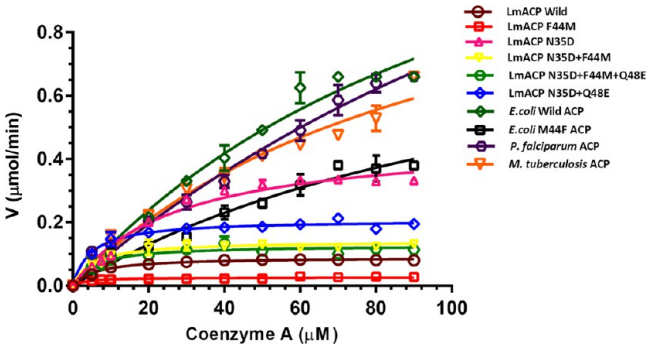

Figure 4. Kinetics of the ACP conversion by Sfp (*B. subtilis*). The Sfp-catalyzed transfer of the phosphopantetheine moiety from CoA using various ACPs as substrates, viz., *E. coli* ACP, M44F mutant of *E. coli* ACP, *P. falciparum* ACP, *M. tuberculosis* ACP, wild-type LmACP, and N35D, F44M, N35D+F44M, N35D+Q48E, and N35D+F44M+Q48E mutants of LmACP. The data were fitted to the Michaelis−Menten equation using Graphpad Prism version 6.0. The K_M and k_{cat} values calculated from the graph are listed in Table 1.

4′-Phosphopantetheinyl Transferase of *L. major* (LmPPT) Does Not Show Any Catalytic Activity toward Its Cognate ACP. On the basis of the enzyme kinetic results with AcpS and Sfp, we hypothesized that the interaction interface of LmACP might have evolved convergently with its cognate PPT and might convert efficiently with its own group II 4′-phosphopantetheinyl transferase, a 273-amino acid protein, the only PPT encoded by the *L. major* genome (UniProt entry Q4QCW3).

As shown on a 12% Native-PAGE gel, only 18% conversion of the wild-type LmACP and mutants N35D, F44M, and N35D +F44M to the holo form was observed after incubation for 8 h (Figure 3D, lanes 1−8). The enzyme assay was comprised of 10 μM LmPPT, 40 μM LmACP, 150 μM CoA, and 50 mM Tris-HCl (pH 8.0) at 37 °C. Interestingly, an assay conducted in the absence of LmPPT (Figure 3D, lane 9) also displayed equivalent conversion to holo-LmACP, suggesting that the small amount of the holo product formed is a consequence of LmACP self-pantetheinylation, and not LmPPT catalysis.

LmPPT Efficiently Converts Heterologous Type I and Type II ACPs into Their Holo Forms. The rate of phosphopantetheinylation of other type I and type II ACPs by LmPPT was also followed. Interestingly, an equivalent amount of the enzyme, under the same assay conditions, displayed higher activity toward *H. sapiens* ACP (71% conversion), *P. falciparum* ACP (70%), *M. tuberculosis* ACP (35%), and *E. coli* ACP (45% conversion) after incubation for 3 h. A longer incubation (4 h) resulted in the complete conversion of *H. sapiens* and *P. falciparum* ACP into their holo forms, as shown in Figure 3E.

Chemical Shift Perturbation Studies Suggest a Weak Interaction between LmACP and Sfp. Chemical shifts are sensitive to the changes in the chemical environment, viz.,

Table 1. Kinetic Constants for Sfp (*B. subtilis*) Determined Using Various ACPs as Substrates

ACP	K_M (μM)	k_{cat} (min^{-1})	V_{max} (μmol min^{-1})	k_{cat}/K_M (min^{-1} M^{-1})
LmACP wild type	6.29 ± 0.70	0.05 ± 0.00	0.09 ± 0.00	7949
LmACP F44A	ND[a]	ND[a]	ND[a]	ND[a]
LmACP F44M	3.79 ± 0.84	0.01 ± 0.00	0.03 ± 0.00	2639
LmACP N35D	26.86 ± 3.53	0.23 ± 0.01	0.47 ± 0.02	8563
LmACP N35D+F44M	5.24 ± 1.08	0.07 ± 0.00	0.14 ± 0.01	13359
LmACP N35D+Q48E	4.81 ± 0.72	0.10 ± 0.00	0.21 ± 0.00	20790
LmACP N35D+F44M+Q48E	5.54 ± 1.39	0.06 ± 0.00	0.13 ± 0.00	10830
E. coli ACP wild type	120.4 ± 26.9	0.84 ± 0.12	1.68 ± 0.25	6977
E. coli ACP M44F	130.2 ± 39.9	0.49 ± 0.10	0.98 ± 0.20	3763
P. falciparum ACP	215 ± 63.88	1.15 ± 0.25	2.28 ± 0.51	5349
M. tuberculosis ACP	100.5 ± 26.8	0.62 ± 0.10	1.25 ± 0.20	6169

[a]Not determined.

DOI: 10.1021/acs.biochem.5b00394
Biochemistry 2015, 54, 5632−5645

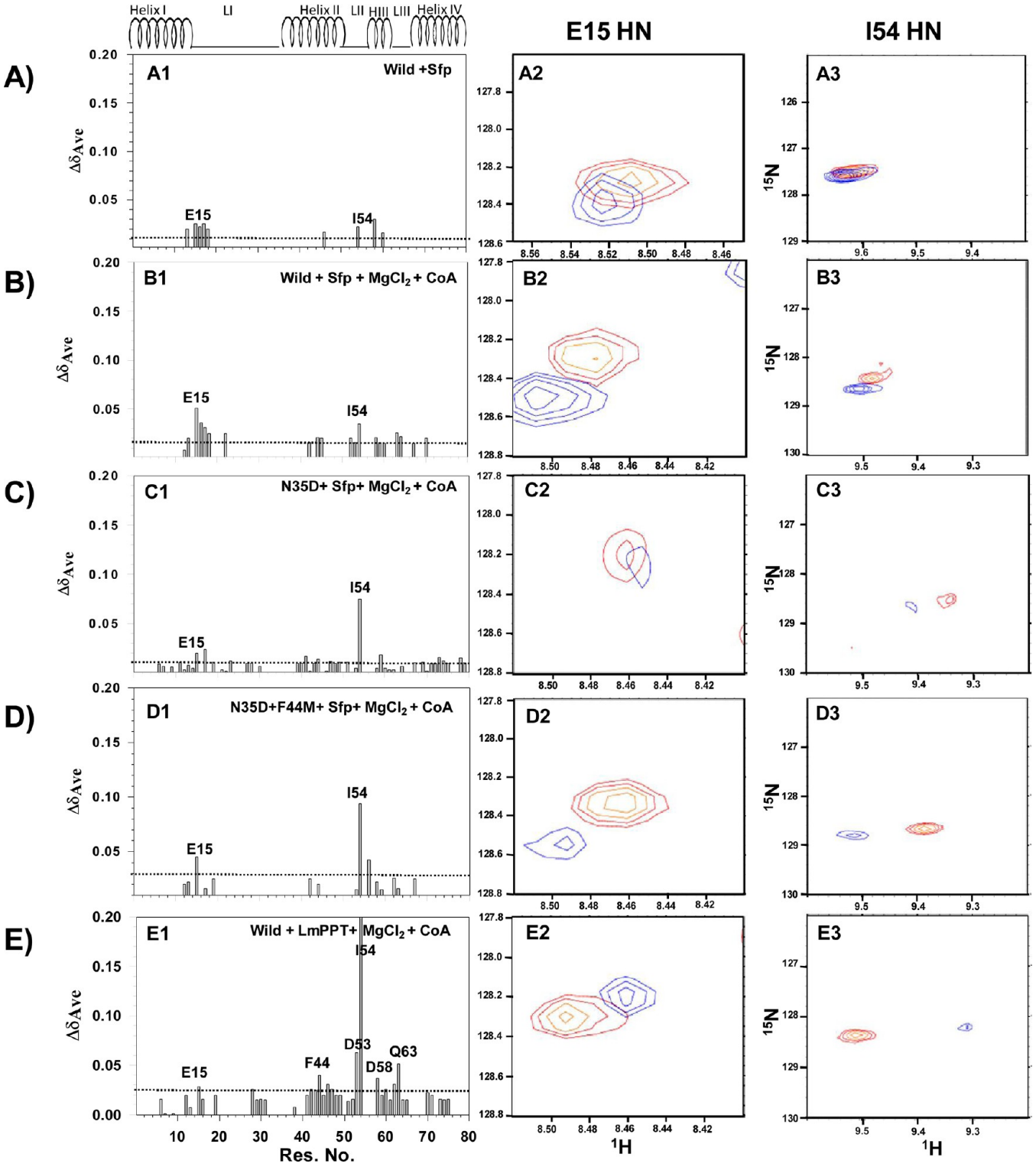

Figure 5. Interaction of LmACP with 4′-phosphopantetheinyl transferase is fairly weak. Average amide chemical shift changes of (A) LmACP upon binding to Sfp alone, (B) LmACP binding to Sfp (*B. subtilis*) in the presence of 2 mM Mg^{2+} and 1.5 mM CoA, (C) the N35D mutant of LmACP upon binding to Sfp in the presence of Mg^{2+} and CoA, (D) the N35D+F44M mutant of LmACP upon binding to Sfp in the presence of Mg^{2+} and CoA, and (E) wild-type LmACP upon binding to LmPPT in the presence of 2 mM Mg^{2+} and 1.5 mM CoA. Panels 2 and 3 display the peaks for Glu 15 and Ile 54 HN, respectively, for titration points at 0-fold (blue) and 2-fold (red) excesses of PPT. A discontinuous line in the figure marks one standard deviation. The binding studies were conducted in 50 mM Tris-HCl (pH 8.0) at 25 °C.

hydrogen bonds, electrostatic interactions, hydrophobic interactions, etc., and, hence, serve as an excellent tool for following ligand interactions.[51] The interaction of LmACP and its mutants with Sfp was also investigated by NMR. All the mutant ACPs appeared to be well-folded in the $^{1}H^{15}N$ HSQC spectra. ^{1}H- and ^{15}N-labeled samples of wild-type LmACP, the N35D mutant, and the double mutant N35D+F44M were titrated with increasing concentrations of unlabeled Sfp, to a final molar ratio of 1:2 in 50

DOI: 10.1021/acs.biochem.5b00394
Biochemistry 2015, 54, 5632−5645

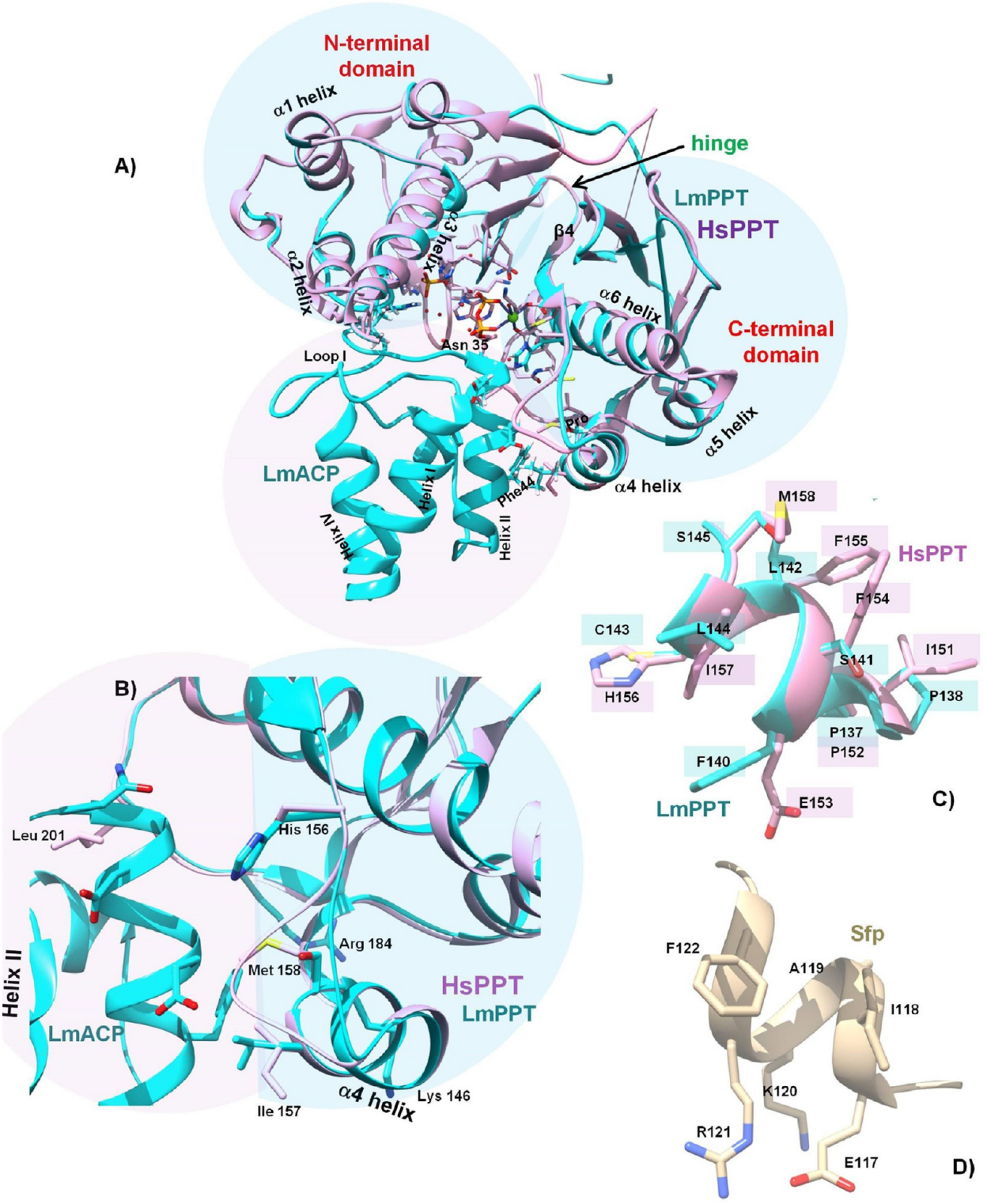

Figure 6. Modeled structure of LmPPT in complex with LmACP. (A) Ribbon representation of the structure of LmPPT (colored cyan) generated using Prime[54] and LmACP (PDB entry 2M5R) colored cyan, based on the HsPPT−ACP complex structure, PDB entry 2CG5 (HsPPT colored pink). Docking was done using Chimera.[57] Residues important for interaction between ACP and PPT are shown as sticks. (B) Comparison of the protein−protein interaction interface between helix α_2 of LmACP (cyan) and helix α_4 of LmPPT (cyan). For comparison, the crystal structure of HsPPT (pink) is also shown, displaying the residues crucial for interaction as sticks: (C) helix α_4 of HsPPT (pink) overlaid on helix α_4 of LmPPT (cyan) and (D) helix α_4 of Sfp (peach).

mM Tris-HCl (pH 8.0) at 25 °C. Figure 5A illustrates the average backbone amide chemical shift changes of LmACP upon addition of Sfp in the absence and Figure 5B in the presence of 2 mM $MgCl_2$ and 1.5 mM CoA. In the former case (Figure 5A1), chemical shift perturbations were restricted to the residues in loop I, and a few residues of helix III. However, in the presence of $MgCl_2$ and CoA (Figure 5B1), perturbations extended to a few more residues in helices II and III of LmACP. Panels C and D of

DOI: 10.1021/acs.biochem.5b00394
Biochemistry 2015, 54, 5632−5645

Figure 5 display chemical shift changes of the amides in the single mutant N35D and the double mutant N35D+F44M, respectively, upon Sfp binding. In all the cases, the chemical shift changes were extremely small, centered around (a) Glu 15 and (b) Ile 54 amides. The amide peaks for residues Glu 15 and Ile 54 in the HSQC spectrum for each titration, in the free LmACP (colored blue) and PPT-bound state (colored red), are displayed in panels 2 and 3, respectively. Interestingly, in our $^{1}H^{15}N$ HSQC experiments, over a period of time, the formation of holo-LmACP could be observed in the single mutant N35D, validating our assumptions that the conformational changes observed in LmACP upon Sfp binding are functionally relevant.

LmACP Forms a Relatively Tight Complex with LmPPT. The chemical shift changes upon binding of LmACP with its cognate PPT (unlabeled) were similar to those observed with Sfp (Figure 5E1). Interestingly, a few more amides in helix II, loop II, and helix III of LmACP, viz., Phe 44, Ile 46, Asp 53, Asp 58, Ile 62, and Gln 63, displayed a noticeable chemical shift change, in addition to Glu 15 and Ile 54 HN. Chemical shift perturbations were observed for hydrophobic as well as charged residues. The direction of the chemical shift change of Ile 54 HN upon interaction with LmPPT was ∼0.4 ppm downfield. Panels A−C of Figure S5 show some of the LmACP peaks in the $^{1}H^{15}N$ HSQC spectrum that experience changes in chemical shift upon titration with LmPPT.

The LmACP−LmPPT interaction was also investigated by following the changes in the $^{1}H^{13}C$ correlation peaks in the $^{1}H^{13}C$ HSQC spectrum of LmACP upon LmPPT binding (Figure S6). Minor changes in the H_{α} chemical shift were observed for Glu 41, Val 43−Glu 47, Ile 54−Ala 59, Lys 61, Tyr 71, and Ile 72 in LmACP. Changes in the H_{β} chemical shift were observed for the residues present in helix I, helix II, loop II, helix III, and loop III (Figure S6B). The γ-protons of only two hydrophobic residues displayed a perceptible change, Val 42 and Leu 52, as shown in Figure S6C.

Sfp-Catalyzed Conversion of Apo-LmACP Is Significantly Reduced in the Presence of LmPPT. The Sfp assay was conducted using 10 μM Sfp, and 40 μM LmACP as a substrate, in the presence of 1-fold (40 μM) and 2-fold (80 μM) molar excesses of LmPPT. Approximately, a 20% reduction in holo-LmACP product was observed in the presence of a 1-fold molar excess (Figure 3F, lane 3) and a 40% reduction with a 2-fold excess of LmPPT (Figure 3F, lane 4). Similar addition of 2- and 4-fold excesses of LmPPT to the Sfp assay using *E. coli* apo-ACP as a substrate did not cause any reduction in the extent of product formation (data not shown). Addition of >500 μM NaCl to the assay mixture did not have any effect on the rate of conversion of LmACP by Sfp in the presence of LmPPT (data not shown).

LmACP Does Not Affect the Conversion of Non-cognate ACPs by LmPPT. LmPPT assays were conducted using *E. coli* and *P. falciparum* ACP as substrates (40 μM), in the presence of LmACP (10 μM). As illustrated in Figure 3G, no change in the *P. falciparum* holo-ACP product was observed in the presence of 80 μM (2-fold molar excess) or 160 μM (4-fold molar excess) LmACP (Figure 3G, lanes 3 and 4).

Insights into the LmACP−LmPPT Interaction from *in Silico* Studies. To understand the interaction of LmACP with its cognate PPT at the molecular level, structure prediction of LmPPT was conducted using three different types of software: I-TASSER,[52] Modeler,[53] and Prime[54] (Schrodinger). The top two models selected by the three types of software were in good agreement and were based on the templates (a) *B. subtilis* Sfp structure (PDB entry 1QR0) and (b) *H. sapiens* PPT (HsPPT, PDB entry 2C43), both displaying ∼20% sequence identity to LmPPT. Evaluation of the stereochemical quality of the generated structures was conducted using PROCHECK,[55] RAMPAGE (mordred.bioc.cam.ac.uk/∼rapper/rampage.php), PSVS[56] (http:/psvs-1_4-dev.nesg.org), MolProbity, Verify3D, ERRAT (available at services.mbi.ucla.edu/SAVES), etc. On the basis of the structure quality factors, the model generated by Prime (Schrodinger) (template 2C43) was selected as the most suitable model. The overall statistics of the structure quality factors for the best three models are illustrated in Supplementary Table 2.

The LmACP molecule (PDB entry 2M5R) was docked on the modeled structure of LmPPT generated by Prime,[54] using the ACP−PPT complex structure as a template (PDB entry 2CG5, 2.7 Å resolution) by automated docking, using the Needleman−Wunsch algorithm of Chimera.[57]

The modeled structure of LmPPT suggests an Sfp-like (*B. subtilis*) or HsPPT-like α/β fold, comprising two identical domains, N- and C-termini, connected by a hinge region as shown in Figure 6A. The sequence of LmPPT is slightly longer than that of HsPPT, and the extra residues lie at the N- and C-termini. Comparison of the LmPPT structure with HsPPT[58] and Sfp[59] suggests that the residues important for catalysis are fully conserved, i.e., a Glu at position 151 in *B. subtilis* Sfp (Glu 171 in LmPPT and Glu 191 in HsPPT) that deprotonates the hydroxyl group of the serine side chain of the incoming ACP, Asp 107 (Asp 128 in LmPPT and Asp 139 in HsPPT) present in the β-sheet to which the hydroxyl group is transferred (residue that forms a coordinate bond with Mg^{2+}), and Lys 155 (Lys 175 in LmPPT and Lys 195 in HsPPT) that transfers it to the oxygen of the α-phosphate. Likewise, the residues involved in Mg^{2+} binding, viz., Asp 129 and Glu 181 in HsPPT, are also conserved in LmPPT, and the corresponding residues are Asp 128 and Glu 171 in the latter protein. The residues that interact with CoA are also similar to some extent; i.e., Arg 57, Arg 96, and His 121 in HsPPT are substituted with Lys 56, Thr 90, and His 110, respectively, in LmPPT. Lys 112 is an important residue, present in the loop preceding helix α_4 in Sfp. In LmPPT, this Lys residue is substituted with a positively charged histidine.

HsPPT interacts with the ACP molecule via its three hydrophobic patches in the crystal structure: (a) Leu 201, (b) the loop between helices α_1 and α_2, involving residues Phe 61−Ala 64, and (c) helix α_4 comprising residues Phe 154−Met 158,[58] and residues Phe 183 and Trp 187. Leucine 181 is conserved in LmPPT, corresponding to position 201 in HsPPT and position 161 in Sfp. Similarly, Phe 163 and Trp 167 in LmPPT correspond to Phe 143 and Trp 147 in Sfp and Phe 183 and Trp 187 in HsPPT, respectively. However, the two hydrophobic patches of PPT that contact two different sides of the ACP molecule are remarkably different in LmPPT, i.e., the loop between helices α_1 and α_2 of PPT that contacts loop I of ACP and helix α_4 that interacts with helix II of ACP. In Sfp, three charged residues, present in helix α_4, namely, Glu 117, Lys 120, and Arg 121,[60] participate in electrostatic interactions with the ACP molecule (Figure S7). In HsPPT, the corresponding residues are Glu 153, His 156, and Lys 159, while in LmPPT, loop α_4 is relatively hydrophobic, where the equivalent residues are Phe 140, Cys 143, and Lys 146, respectively (Figure 6C,D).

DISCUSSION

In this study, we have determined the structure of the holo-acyl carrier protein of *L. major* and studied its interactions with two

DOI: 10.1021/acs.biochem.5b00394
Biochemistry 2015, 54, 5632−5645

groups of widely used 4′-phosphopantetheinyl transferases, bacterial group I (AcpS) and group II (Sfp from *B. subtilis*). Our studies shed light on the unique interaction surface of LmACP, which has probably evolved to interact with its cognate PPT. The versatility of NMR spectroscopy, coupled with biochemical studies, offered unique opportunities to understand the structure, backbone dynamics, kinetics, and ligand interactions of LmACP, which combined together divulged interesting details regarding its function.

Sequence identity and structural homology of LmACP categorizes it as a type II ACP involved in fatty acid biosynthesis. With the *E. coli* ACP sequence, it shows 39% identity, 34% with *P. falciparum* ACP, and 45% with the *H. sapiens* mitochondrial ACP (PDB entry 2DNW). Structurally, the LmACP molecule comprises four helices, I–IV, enclosing a large hydrophobic cleft. Residues crucial for acyl chain sequestration are conserved, viz., Phe 28, Ser 36, Val 39, Ile 46, and Ile 54, suggesting a function similar to those of other type II ACPs. Biochemical studies using Sfp from *B. subtilis* confirm that LmACP is functional and can undergo post-translational modification at the conserved Ser residue to form holo-LmACP.

A disparity in sequence, however, exists between LmACP and other type II ACPs, at positions known to interact with PPTs. The "DSL motif" of the type II ACPs is substituted with an NSL motif in LmACP. Similar nonconservation of the motif has been observed in the type I ACP of *Streptomyces sioyaensis* and *Streptomyces laurentii*,[46] where a TSL motif has been observed, an HSL motif in PCPs, and a DSI motif in *E. coli* strain O157:H7.[46] Another important position is 44, conserved in most type II ACPs. The Met at this position is replaced with a Phe in LmACP. The importance of an Asp at position 35 and a methionine at position 44 in type II ACPs has been elucidated in the X-ray cocrystal structure of the ACP–AcpS (4′-phosphopantetheinyl transferase) complex of *B. subtilis*, which has served as a prototype to understand the molecular mechanism of phosphopantetheinylation by PPT in general.[61] In the ACP–AcpS complex, the side chains of Leu 37 and Met 44 of ACP interact with the AcpS molecule, stretching into the hydrophobic pocket, interacting with Met 18, Gln 22, Phe 25, Arg 28, and Phe 54 of AcpS. Likewise, Asp 35 of ACP is involved in a salt bridge with Arg 14 of AcpS, and Glu 41 with Arg 21.[61] As positions 35 and 44 are occupied by an Asn and a Phe, respectively, in LmACP, extremely low AcpS activity was observed with wild-type LmACP (1%), upon heterologous expression in *E. coli*. On the other hand, the double mutant N35D+F44M displayed 17% conversion to the holoprotein, underscoring the stringent residue requirement of AcpS for activity. Likewise, the triple mutant N35D+F44M+Q48E also displayed similar conversion to holo-LmACP upon expression in *E. coli*, analogous to that of the double mutant N35D+F44M. The genome of *Leishmania* lacks any AcpS type, group I phosphopantetheinyl transferase, unlike *P. falciparum*[46] and *M. tuberculosis*,[46] and hence, the residues crucial for interaction with AcpS may not have been selected by nature.

Position 35 is important for the interaction of ACP with Sfp, a group II PPT, as well. Salt bridges have been thought to exist between Lys 112 of Sfp and aspartates 35 and 38 of ACP, based on the superposition of the ACP–AcpS complex structure on the Sfp molecule, and the identification of the equivalent residues in Sfp.[61,62] A prior mutagenesis study of an acyl carrier protein domain from a modular polyketide synthase elucidated the importance of the aspartate at position 35 in the phosphopantetheinylation of ACP by Sfp.[63] In sync with the previous report, the rate of turnover of wild-type LmACP (NSL motif) into its holo form by Sfp was 16-fold lower than that of *E. coli* ACP in our studies. The single mutant N35D of LmACP displayed a k_{cat} ~5 times higher than that of wild-type LmACP. Notably, the k_{cat} of LmACP mutant N35D is still ~4-fold lower than that of *E. coli* ACP, suggesting that some other factors, in addition to the NSL motif, also contribute to the differences in k_{cat}.

Besides the DSL motif, the hydrophobic interactions also play a crucial role in the ACP–Sfp interaction. From our biochemical studies, some basic rules that govern the promiscuity of Sfp became apparent. Mutation of Phe 44 to an Ala limited promiscuous catalysis of LmACP by Sfp. No product was formed even after incubation for several hours. Interestingly, in a few carrier proteins, i.e., Frenolicin N-ACP molecule,[64] TycC3-PCP,[65] and *Saccharomyces coelicolor* ACP,[46] an alanine is naturally present at position 44, and the Sfp molecule accepts them as a substrate, converting them into holo-ACP. Notably, in the three aforementioned proteins, the residue at position 40, $i-4$ to Ala 44, are long chain hydrophobic residues, viz., Leu, Met, and Met, respectively, that interact with the hydrophobic patch of Sfp. In the F44A mutant of LmACP, a Val is present at position 40 and an Ala at position 44. These observations, along with insights from the crystal structure of the Sfp-PCP complex,[59] and comparison with other carrier proteins efficiently converted by Sfp suggest that positions 37 (site A), 40 (site B), and 44 (site C) (Figure 2) present in the helix II of ACP are important determinants of its interaction with Sfp via hydrophobic interactions. In all carrier proteins, (site A) position 37 is invariably a Leu/Ile, because of the conservation of the DSL/HSL/TSL/DSI motif. Thus, sites B and C of most ACPs make a difference in their interaction with Sfp. In ACPs, where both sites B and C are occupied by short hydrophobic side chains, e.g., Val, as in *M. tuberculosis* type II ACP, the need for a longer hydrophobic side chain does not arise. However, if site B or site C is an alanine, or a short polar residue, e.g., Ser, as in *Streptococcus pneumoniae* ACP, the other position should necessarily be a longer side chain (e.g., Phe) to make optimal contacts with the hydrophobic residues of Sfp, viz., Phe 154–Met 158,[59] Phe 183, and Trp 187 of Sfp. Conceivably, the arrangement of the hydrophobic residues of Sfp with respect to the ACP molecule, in the ACP–Sfp complex, is predetermined by the distribution of hydrophobic residues on helix II of a given carrier protein. The hinge region between the two domains of Sfp additionally contributes to promiscuity, by imparting flexibility to the C-terminal domain, allowing it to change its orientation and/or position based on the arrangement of the hydrophobic residues on the carrier protein. Beyond position 44, the residues of helix II that participate in electrostatic interactions with Sfp are polar and/or charged. This hypothesis is corroborated by the activity of Sfp toward short peptide tags:[66,67] peptides S1–S7 (S1, GDSLSWLVRCLN) and ybbR13 (DSLEFIASKLA). In these peptides, Leu 44 has been observed to be extremely important for catalysis by Sfp, as the peptides extended by nine residues beyond Ser 36 only show activity. Shorter peptide tags with four or five residues missing at the C-terminal region fail to convert to product.

Another factor that seems important in Sfp–ACP interaction is shape complementarity. The same residue, at the same position in two different ACPs, contributes differently to catalysis. In *E. coli* ACP, a methionine at position 44 gave a low K_M and a high V_{max} with Sfp, while the same residue resulted in a drastic decrease in V_{max} in LmACP. Likewise, a Phe at the same position in *E. coli* resulted in a K_M much higher than that of a Met, while in

DOI: 10.1021/acs.biochem.5b00394
Biochemistry 2015, 54, 5632–5645

LmACP, it was vice versa. In the triple mutant N35D+F44M +Q48E, the surface of helix II of LmACP is exactly similar to that of *E. coli*, yet the V_{max} of this mutant was ~13-fold lower than that of *E. coli* ACP. Possibly, the overall shape of the carrier protein (in addition to the arrangement of the critical residues) dictates its binding to the cleft between the two domains of Sfp, akin to *H. sapiens* PPT (HsPPT).[58] Notably, the double mutant N35D +F44M and the triple mutant N35D+F44M+Q48E of LmACP, which display low V_{max} values with Sfp, are efficiently converted by AcpS *in vivo*, emphasizing the fundamental differences in the mechanism of recognition by the two different groups of 4′-phosphopantetheinyl transferases, AcpS, and Sfp.

Sfp follows a bisubstrate mechanism, binding two substrates, ACP and CoA, at two different sites, resulting in a ternary complex. The initial rates for a bisubstrate mechanism as a function of substrate concentration can be represented by the Cleland equation:[68]

$$v = V_{max}[A][B]/K_d^{A}K_M^{B} + K_M^{B}[A] + K_M^{A}[B] + [A][B]$$

where K_d^{A} is the dissociation constant for the EA complex and K_M^{A} and K_M^{B} are the Michaelis constants for substrates A and B, respectively. However, at a fixed concentration of ACP, as used in our studies (40 μM), the enzyme seems to obey the Michaelis–Menten equation with an increasing CoA concentration. The equation for the bisubstrate reaction can be simplified to

$$v = V_{max}[A]/K_M^{A} + [A]$$

and the results can be interpreted in light of the Michaelis–Menten equation. Thus, the low V_{max}, i.e., (E × k_2), of Sfp for CoA using wild-type LmACP and its mutants compared to those of *E. coli*, *P. falciparum*, and *M. tuberculosis* ACP suggests that the catalytic step involving the conversion of the enzyme–substrate complex into product (k_2) is altered in the equation shown below:

$$E + A \underset{k_{-1}}{\overset{k_1}{\rightleftharpoons}} EA \xrightarrow{k_2} E + P$$

Similarly, in the *E. coli* mutant M44F, K_M remains unaltered but V_{max} decreases. We speculate that in both cases, either the enzyme spends a large part of the time searching for favorable conformation or the enzyme–substrate complex dissociates slowly into product. All the mutations (except N35D) have been introduced in helix II of ACP, at sites involved in protein–protein interaction with Sfp, remote (>10 Å) from the catalytic residues of Sfp.

NMR chemical shift perturbation studies provide additional insights into the nature of the ACP–Sfp interaction. The overall small magnitude of the amide chemical shift changes in LmACP upon Sfp binding offers a window into the fairly weak and transient nature of the interaction, which is probably necessary for the timely release of the substrate and end products. Chemical shift changes were observed at two sites: (a) residues surrounding Glu 15 and (b) residues surrounding Ile 54 HN. The balance appeared to tip in favor of either of these sites in wild-type LmACP and the mutants. In wild-type LmACP, the chemical shift changes were larger for Glu 15 amide, while in the single mutant N35D, and the double mutant N35D+F44M, Ile 54 HN displayed a much larger change. The two sites interact with two different domains of the pseudo-dimer of Sfp, attached by a flexible hinge region.[59] Thus, the data indirectly point toward the rearrangement of the two domains of Sfp with respect to LmACP, to attain a preferred conformation, that ultimately determines the activity of Sfp toward CoA.

The structural insights gained from the modeled structure of LmPPT, combined with the NMR studies, offer an explanation for the lack of enzymatic activity displayed by LmPPT toward its cognate LmACP. The similarity in the pattern of the chemical shift changes of LmACP upon binding LmPPT and Sfp suggests that LmACP binds the active site of LmPPT, between the two domains of the pseudo-dimer. The addition of a 2-fold molar excess of LmPPT to the Sfp assay slowed the enzymatic conversion of LmACP by 40%, supporting the formation of the LmACP–LmPPT complex. However, the addition of 2- and 4-fold molar excesses of LmACP to the LmPPT assay did not cause any decrease in the level of *P. falciparum* or *E. coli* holo-ACP formation. We speculate that the active site of LmPPT either is accessible to the noncognate substrates in the LmPPT–LmACP complex or becomes available by the displacement of LmACP with noncognate ACPs. Hydrophobic, polar, and charged residues of helices II and III of LmACP seem to contribute to this interaction, as revealed by the changes in chemical shift. Comparison of the LmPPT model with the crystal structure of Sfp and HsPPT suggests that the charged residues, Glu 153 and His 156 present in helix α_4 of HsPPT (Figure 6C,D), equivalent to Glu 117 and Arg 121 in Sfp, respectively, that interact with helix II of ACP, are substituted with Phe 140 and Cys 143 in LmPPT, respectively, making the α_4 helix of LmPPT extremely hydrophobic. The hydrophobicity of helix α_4, coupled with the presence of positively charged residues in LmPPT, in the vicinity of helix III of LmACP in the LmACP–LmPPT complex, i.e., Lys 146 in the loop following helix α_4, and Arg 184 in the loop following helix α_6 (Figure 6C), could lead to improper binding of LmACP (Figure 6A). Thus, the interplay of hydrophobic and electrostatic interactions collectively contributes to the unique LmACP–LmPPT interaction. As the enzyme displays reasonable activity with other heterologous ACPs but fails to convert its own cognate ACP into product, substrate inhibition seems to be involved, which is also observed in a few other systems, viz., SePPtII, a group II PPT,[63] *E. coli*,[69] *B. subtilis*,[62] and *S. pneumoniae* AcpS,[70] belonging to PPT group I. We speculate that the observed LmPPT inhibition by its cognate LmACP may possibly be a means of regulation in *Leishmania*. Further studies are underway to fully characterize the LmPPT–LmACP interaction at the molecular level.

■ ASSOCIATED CONTENT

Supporting Information

The Supporting Information is available free of charge on the ACS Publications website at DOI: 10.1021/acs.biochem.5b00394.

Comparison of holo-LmACP structure with other ACPs, relaxation parameters for holo-LmACP, elution profiles for ACPs after the PPT assay, MALDI-TOF analysis of LmACP, $^{1}H^{15}N$ HSQC spectra of LmACP upon LmPPT interaction, ^{1}H chemical shift changes upon LmPPT binding, and structure-based sequence alignment of LmPPT (PDF)

■ AUTHOR INFORMATION

Corresponding Author

*National Institute of Immunology, Aruna Asaf Ali Marg, New Delhi 110 067, India. Telephone: +91-11-26703823. Fax: +91 11 26162125. E-mail: monicasundd@nii.res.in.

DOI: 10.1021/acs.biochem.5b00394
Biochemistry 2015, 54, 5632–5645

Author Contributions

A.K. and R.A. contributed equally to this work.

Funding

The work was supported by a grant [Sanction 5/8-7(90)/2010-ECD-II] from the Indian Council of Medical Research to M.S. We thank the Department of Biotechnology, Government of India, for the infrastructure support. Mr. Ambrish Kumar, Ms. Richa Arya, and Ms. Usha Yadav are recipients of a fellowship from the University Grants Commission of India.

Notes

The authors declare no competing financial interest.

■ ACKNOWLEDGMENTS

We thank Mr. Daya Nand (National Institute of Immunology) for purifying some of the proteins and Ms. Sujata Kumari for making the N35D+F44M mutation.

■ ABBREVIATIONS

LmACP, *L. major* acyl carrier protein; FAS, fatty acid synthase; CoA, coenzyme A; PPT, phosphopantetheinyl transferase; Sfp, *B. subtilis* type II phosphopantetheinyl transferase; HsPPT, *H. sapiens* PPT; LmPPT, *L. major* PPT; AcpS, bacterial type I phosphopantetheinyl transferase.

■ REFERENCES

(1) Croft, S. L., Sundar, S., and Fairlamb, A. H. (2006) Drug resistance in leishmaniasis. *Clin. Microbiol. Rev. 19*, 111−126.

(2) Maltezou, H. C. (2010) Drug resistance in visceral leishmaniasis. *J. Biomed. Biotechnol. 2010*, 617521.

(3) Mutiso, J. M., Macharia, J. C., Kiio, M. N., Ichagichu, J. M., Rikoi, H., and Gicheru, M. M. (2013) Development of Leishmania vaccines: predicting the future from past and present experience. *J. Biomed. Res. 27*, 85−102.

(4) Mbongo, N., Loiseau, P. M., Billion, M. A., and Robert-Gero, M. (1998) Mechanism of amphotericin B resistance in Leishmania donovani promastigotes. *Antimicrob. Agents Chemother. 42*, 352−357.

(5) Coombs, G. H., Craft, J. A., and Hart, D. T. (1982) A comparative study of Leishmania mexicana amastigotes and promastigotes. Enzyme activities and subcellular locations. *Mol. Biochem. Parasitol. 5*, 199−211.

(6) Berman, J. D., Gallalee, J. V., Best, J. M., and Hill, T. (1987) Uptake, distribution, and oxidation of fatty acids by Leishmania mexicana amastigotes. *J. Parasitol. 73*, 555−560.

(7) Hee Lee, S. H., Stephens, J. L., and Englund, P. T. (2007) A fatty-acid synthesis mechanism specialized for parasitism. *Nat. Rev. Microbiol. 5*, 287−297.

(8) Rosenzweig, D., Smith, D., Opperdoes, F., Stern, S., Olafson, R. W., and Zilberstein, D. (2007) Retooling Leishmania metabolism: from sand fly gut to human macrophage. *FASEB J. 22*, 590−602.

(9) Gurvitz, A. (2009) Identification of the Leishmania major proteins LmjF07.0430, LmjF07.0440 and LmjF27.2440 as components of Fatty acid synthase II. *J. Biomed. Biotechnol. 2009*, 950864.

(10) Stephens, J. L., Lee, S. H., Paul, K. S., and Englund, P. T. (2007) Mitochondrial Fatty acid synthesis in Trypanosoma brucei. *J. Biol. Chem. 282*, 4427−4436.

(11) Waller, R. F., Ralph, S. A., Reed, M. B., Su, V., Douglas, J. D., Minnikin, D. E., Cowman, A. F., Besra, G. S., and McFadden, G. I. (2003) A type II pathway for fatty acid biosynthesis presents drug targets in Plasmodium falciparum. *Antimicrob. Agents Chemother. 47*, 297−301.

(12) Lamichhane, G. (2011) Novel targets in M. tuberculosis: search for new drugs. *Trends Mol. Med. 17*, 25−33.

(13) Cronan, J. E., Jr. (1982) Molecular properties of short chain acyl thioesters of acyl carrier protein. *J. Biol. Chem. 257*, 5013−5017.

(14) Reed, M. A., Schweizer, M., Szafranska, A. E., Arthur, C., Nicholson, T. P., Cox, R. J., Crosby, J., Crump, M. P., and Simpson, T. J. (2003) The type I rat fatty acid synthase ACP shows structural homology and analogous biochemical properties to type II ACPs. *Org. Biomol. Chem. 1*, 463−471.

(15) White, S. W., Zheng, J., Zhang, Y. M., and Rock, C. O. (2005) The structural biology of type II fatty acid biosynthesis. *Annu. Rev. Biochem. 74*, 791−831.

(16) Shen, B., Summers, R. G., Gramajo, H., Bibb, M. J., and Hutchinson, C. R. (1992) Purification and characterization of the acyl carrier protein of the Streptomyces glaucescens tetracenomycin C polyketide synthase. *J. Bacteriol. 174*, 3818−3821.

(17) Summers, R. G., Ali, A., Shen, B., Wessel, W. A., and Hutchinson, C. R. (1995) Malonyl-coenzyme A: Acyl Carrier Protein acyltransferase of Streptomyces glaucescens: a possible link between fatty acid and polyketide biosynthesis. *Biochemistry 34*, 9389−9402.

(18) Epple, G., van der Drift, K. M. G. M., Thomas-Oates, J. E., and Geiger, O. (1998) Characterization of a novel acyl carrier protein, RkpF, encoded by an operon involved in capsular polysaccharide biosynthesis in Sinorhizobium meliloti. *J. Bacteriol. 180*, 4950−4954.

(19) Kleinkauf, H., and von Dohren, H. (1990) Nonribosomal biosynthesis of peptide antibiotics. *Eur. J. Biochem. 192*, 1−15.

(20) Stein, T., Vater, J., Kruft, V., Otto, A., Wittmann-Liebold, B., Franke, P., Panico, M., McDowell, R., and Morris, H. R. (1996) The multiple carrier model of nonribosomal peptide biosynthesis at modular multienzymatic templates. *J. Biol. Chem. 271*, 15428−15435.

(21) Roujeinikova, A., Simon, W. J., Gilroy, J., Rice, D. W., Rafferty, J. B., and Slabas, A. R. (2007) Structural studies of fatty acyl-(acyl carrier protein) thioesters reveal a hydrophobic binding cavity that can expand to fit longer substrates. *J. Mol. Biol. 365*, 135−145.

(22) Masoudi, A., Raetz, C. R. H., Zhou, P., and Pemble, C. W., IV (2013) Chasing acyl carrier protein through a catalytic cycle of lipid A production. *Nature 505*, 422−426.

(23) Nguyen, C., Haushalter, R. W., Lee, D. J., Markwick, P. R. L., Bruegger, J., Caldara-Festin, G., Finzel, K., Jackson, D. R., Ishikawa, F., O'Dowd, B., McCammon, J. A., Opella, S. J., Tsai, S. C., and Burkart, M. D. (2013) Trapping the dynamic acyl carrier protein in fatty acid biosynthesis. *Nature 505*, 427−431.

(24) Zornetzer, G. A., Fox, B. G., and Markley, J. L. (2006) Solution structures of spinach acyl carrier protein with decanoate and stearate. *Biochemistry 45*, 5217−5227.

(25) Sharma, A. K., Sharma, S. K., Surolia, A., Surolia, N., and Sarma, S. P. (2006) Solution structures of conformationally equilibrium forms of holo-acyl carrier protein (PfACP) from Plasmodium falciparum provides insight into the mechanism of activation of ACPs. *Biochemistry 45*, 6904−6916.

(26) Upadhyay, S. K., Misra, A., Srivastava, R., Surolia, N., Surolia, A., and Sundd, M. (2009) Structural Insights into the acyl intermediates of the Plasmodium falciparum fatty acid synthesis pathway: the mechanism of expansion of the acyl carrier protein core. *J. Biol. Chem. 284*, 22390−22400.

(27) Gallagher, J. R., and Prigge, S. T. (2010) Plasmodium falciparum acyl carrier protein crystal structures in disulfide-linked and reduced states and their prevalence during blood stage growth. *Proteins: Struct., Funct., Genet. 78*, 575−588.

(28) Ploskon, E., Arthur, C. J., Evans, S. E., Williams, C., Crosby, J., Simpson, T. J., and Crump, M. P. (2008) A mammalian type I fatty acid synthase acyl carrier protein domain does not sequester acyl chains. *J. Biol. Chem. 283*, 518−528.

(29) Chan, D. I., Chu, B. C., Lau, C. K., Hunter, H. N., Byers, D. M., and Vogel, H. J. (2010) NMR solution structure and biophysical characterization of Vibrio harveyi acyl carrier protein A75H: effects of divalent metal ions. *J. Biol. Chem. 285*, 30558−30566.

(30) Agarwal, V., Lin, S., Lukk, T., Nair, S. K., and Cronan, J. E. (2012) Structure of the enzyme-acyl carrier protein (ACP) substrate gatekeeper complex required for biotin synthesis. *Proc. Natl. Acad. Sci. U. S. A. 109*, 17406−17411.

(31) Babu, M., Greenblatt, J. F., Emili, A., Strynadka, N. C., Reithmeier, R. A., and Moraes, T. F. (2010) structure of a SLC26 anion transporter STAS domain in complex with acyl carrier protein: Implications for E. coli YchM in fatty acid metabolism. *Structure 18*, 1450−1462.

DOI: 10.1021/acs.biochem.5b00394
Biochemistry 2015, 54, 5632−5645

(32) Kumar, A., Surolia, A., and Sundd, M. (2012) Backbone and side chain 1H, 15N and 13C chemical shift assignments of the holo-acyl carrier protein (ACP) of Leishmania major. *Biomol. NMR Assignments 6*, 221−223.
(33) Lambalot, R. H., and Walsh, C. T. (1995) Cloning, overproduction, and characterization of the Escherichia coli holo-acyl carrier protein synthase. *J. Biol. Chem. 270*, 24658−24661.
(34) Delaglio, F., Grzesiek, S., Vuister, G. W., Zhu, G., Pfeifer, J., and Bax, A. (1995) NMRPipe: a multidimensional spectral processing system based on UNIX pipes. *J. Biomol. NMR 6*, 277−293.
(35) Goddard, T. D., and Kneller, D. G. (2012) *SPARKY 3*, University of California, San Francisco.
(36) Keller, R. L. J. (2004) Optimizing the process of nuclear magnetic resonance spectrum analysis and computer aided resonance assignment. Ph.D. Thesis, ETH Zurich, Zurich.
(37) Wishart, D. S., Bigam, C. G., Yao, J., Abildgaard, F., Dyson, H. J., Oldfield, E., Markley, J. L., and Sykes, B. D. (1995) 1H, 13C and 15N chemical shift referencing in Biomolecular NMR. *J. Biomol. NMR 6*, 135−140.
(38) Raiford, D. S., Fisk, C. L., and Becker, E. D. (1979) Calibration of methanol and ethylene glycol nuclear magnetic resonance thermometers. *Anal. Chem. 51*, 2050−2051.
(39) Chill, J. H., Louis, J. M., Miller, C., and Bax, A. (2006) NMR study of the tetrameric KcsA potassium channel in detergent micelles. *Protein Sci. 15*, 684−698.
(40) Cole, R., and Loria, P. J. (2003) FAST-Modelfree: A program for rapid automated analysis of solution NMR spin-relaxation data. *J. Biomol. NMR 26*, 203−213.
(41) Brunger, A. T., Adams, P. D., Clore, G. M., DeLano, W. L., Gros, P., Grosse-Kunstleve, R. W., Jiang, J. S., Kuszewski, J., Nilges, M., Pannu, N. S., Read, R. J., Rice, L. M., Simonson, T., and Warren, G. L. (1998) Crystallography & NMR system: A new software suite for macromolecular structure determination. *Acta Crystallogr., Sect. D: Biol. Crystallogr. 54*, 905−921.
(42) Nair, D. R., Ghosh, R., Manocha, A., Mohanty, D., Saran, S., and Gokhale, R. S. (2011) Two functionally distinctive phosphopantetheinyl transferases from amoeba Dictyostelium discoideum. *PLoS One 6*, e24262.
(43) Mootz, H. D., Finking, R., and Marahiel, M. A. (2001) 4′-Phosphopantetheine transfer in primary and secondary metabolism of Bacillus subtilis. *J. Biol. Chem. 276*, 37289−37298.
(44) Shen, Y., Delaglio, F., Cornilescu, G., and Bax, A. (2009) TALOS +: A hybrid method for predicting protein backbone torsion angles from NMR chemical shifts. *J. Biomol. NMR 44*, 213−223.
(45) Clore, G. M., Szabo, A., Bax, A., Kay, L. E., Driscoll, P. C., and Gronenborn, A. M. (1990) Deviations from the simple two-parameter model-free approach to the interpretation of nitrogen-15 nuclear magnetic resonance of proteins. *J. Am. Chem. Soc. 112*, 4989−4991.
(46) Beld, J., Sonnenschein, E. C., Vickery, C. R., Noel, J. P., and Burkart, M. D. (2014) The phosphopantetheinyl transferases: catalysis of a post-translational modification crucial for life. *Nat. Prod. Rep. 31*, 61−108.
(47) Hill, R. B., MacKenzie, K. R., Flanagan, J. M., Cronan, J. E., Jr., and Prestegard, J. H. (1995) Overexpression, purification and characterization of Escherichia coli acyl carrier protein and two mutant proteins. *Protein Expression Purif. 6*, 394−400.
(48) Sharma, S. K., Modak, R., Sharma, S., Sharma, A. K., Sarma, S. P., Surolia, A., and Surolia, N. (2005) A novel approach for over-expression, characterization, and isotopic enrichment of a homogeneous species of acyl carrier protein from Plasmodium falciparum. *Biochem. Biophys. Res. Commun. 330*, 1019−1026.
(49) Broadwater, J. A., and Fox, B. G. (1999) Spinach holo-acyl carrier protein: overproduction and phosphopantetheinylation in Escherichia coli BL21(DE3), *in vitro* acylation, and enzymatic desaturation of histidien-tagged isoform I. *Protein Expression Purif. 15*, 314−326.
(50) Morris, S. A., Revill, W. P., Staunton, J., and Leadlay, P. F. (1993) Purification and separation of holo- and apo- forms of Saccharopolyspora erythraea acyl-carrier protein released from recombinant Escherichia coli by freezing and thawing. *Biochem. J. 294* (Part 2), 521−527.
(51) Williamson, M. P. (2013) Using chemical shift perturbation to characterize ligand binding. *Prog. Nucl. Magn. Reson. Spectrosc. 73*, 1−16.
(52) Roy, A., Kucukural, A., and Zhang, Y. (2010) I-TASSER: a unified platform for automated protein structure and function prediction. *Nat. Protoc. 5*, 725−738.
(53) Eswar, N., Eramian, D., Webb, B., Shen, M.-Y., and Sali, A. (2008) Protein structure modeling with MODELLER. *Methods Mol. Biol. 426*, 145−159.
(54) Jacobson, M. P., Pincus, D. L., Rapp, C. S., Day, T. J. F., Honig, B., Shaw, D. E., and Friesner, R. A. (2004) A hierarchical approach to all-atom protein loop prediction. *Proteins: Struct., Funct., Genet. 55*, 351−367.
(55) Laskowski, R. A., MacArthur, M. W., Moss, D. S., and Thornton, J. M. (1993) PROCHECK-a program to check the stereochemical quality of protein structures. *J. Appl. Crystallogr. 26*, 283−291.
(56) Bhattacharya, A., Tejero, R., and Montelione, G. T. (2007) Evaluating protein structures determined by structural genomics consortia. *Proteins: Struct., Funct., Genet. 66*, 778−795.
(57) Pettersen, E. F., Goddard, T. D., Huang, C. C., Couch, G. S., Greenblatt, D. M., Meng, E. C., and Ferrin, T. E. (2004) UCSF Chimera- a visualization system for exploratory research and analysis. *J. Comput. Chem. 25*, 1605−1612.
(58) Bunkoczi, G., Pasta, S., Joshi, A., Wu, X., Kavanagh, K. L., Smith, S., and Oppermann, U. (2007) Mechanism and substrate recognition of human holo ACP synthase. *Chem. Biol. 14*, 1243−1253.
(59) Tufar, P., Rahighi, S., Kraas, F. I., Kirchner, D. K., Lohr, F., Henrich, E., Kopke, J., Dikic, I., Guntert, P., Marahiel, M. A., and Dotsch, V. (2014) Crystal structure of a PCP/Sfp complex reveals the structural basis for carrier protein post-translational modification. *Chem. Biol. 21*, 552−562.
(60) Mofid, M. R., Finking, R., Essen, L. O., and Marahiel, M. A. (2004) Structure-based mutational analysis of the 4′-phosphopantetheinyl transferases Sfp from Bacillus subtilis: Carrier protein recognition and reaction mechanism. *Biochemistry 43*, 4128−4136.
(61) Parris, K. D., Lin, L., Tam, A., Mathew, R., Hixon, J., Stahl, M., Fritz, C. C., Seehra, J., and Somers, W. S. (2000) Crystal structures of substrate binding to Bacillus subtilis holo-(acyl carrier protein) synthase reveal a novel trimeric arrangement of molecules resulting in three active sites. *Structure 8*, 883−895.
(62) Finking, R., Mofid, M. R., and Marahiel, M. A. (2004) Mutational analysis of peptidyl carrier protein and acyl carrier protein synthase unveils residues involved in protein-protein recognition. *Biochemistry 43*, 8946−8956.
(63) Weissman, K. J., Hong, H., Popovic, B., and Meersman, F. (2006) Evidence for a protein-protein interaction motif on an acyl carrier protein domain from a modular polyketide synthase. *Chem. Biol. 13*, 625−636.
(64) Li, Q., Khosla, C., Puglisi, J. D., and Liu, C. W. (2003) Solution structure and backbone dynamics of the holo form of the frenolicin acyl carrier protein. *Biochemistry 42*, 4648−4657.
(65) Weber, T., Baumgartner, R., Renner, C., Marahiel, M. A., and Holak, T. A. (2000) Solution structure of PCP, a prototype for the peptidyl carrier domains of modular peptide synthetases. *Structure 8*, 407−418.
(66) Yin, J., Straight, P. D., McLoughlin, S. M., Zhou, Z., Lin, A. L., Golan, D. E., Kelleher, N. L., Kolter, R., and Walsh, C. T. (2005) Genetically encoded short peptide tag for versatile protein labeling by Sfp phosphopantetheinyl transferase. *Proc. Natl. Acad. Sci. U. S. A. 102*, 15815−15820.
(67) Zhou, Z., Cironi, P., Lin, A. J., Xu, Y., Hrvatin, S., Golan, D. E., Silver, P. A., Walsh, C. J., and Yin, J. (2007) Genetically encoded short peptide tags for orthogonal protein labeling by Sfp and AcpS Phosphopantetheinyl transferases. *ACS Chem. Biol. 2*, 337−346.
(68) Cleland, W. W. (1967) The statistical analysis of enzyme kinetic data. *Adv. Enzymol. Relat. Areas Mol. Biol. 29*, 1−32.
(69) Flugel, R. S., Hwangbo, Y., Lambalot, R. H., Cronan, J. E., Jr., and Walsh, C. T. (2000) Holo-(acyl carrier protein) synthase and

DOI: 10.1021/acs.biochem.5b00394
Biochemistry 2015, 54, 5632−5645

phosphopantetheinyl transfer in Escherichia coli. *J. Biol. Chem. 275*, 959−968.
(70) McAllister, K. A., Peery, R. B., Meier, T. I., Fischl, A. S., and Zhao, G. (2000) Biochemical and molecular analyses of the Streptococcus pneumoniae acyl carrier protein synthase, an enzyme essential for fatty acid biosynthesis. *J. Biol. Chem. 275*, 30864−30872.

DOI: 10.1021/acs.biochem.5b00394
Biochemistry 2015, 54, 5632−5645